Tantalum(V) Nitride Inverse Opals as Photonic Structures for Visible Wavelengths

Alessandro Rugge,[†] Jin-Seong Park,[‡] Roy G. Gordon,*[,‡] and Sarah H. Tolbert*[,†]

Department of Chemistry and Biochemistry, University of California Los Angeles, Los Angeles, California 90095-1569, and Department of Chemistry, Harvard University, Cambridge, Massachusetts 02138

Received: July 2, 2004; In Final Form: September 24, 2004

The development of materials with a complete photonic band gap at visible wavelengths is believed to have the potential to lead to new control over long-lived emissive excited states, single molecule lasers, and nearly lossless nanoscale waveguides. In this work we move toward that goal with the synthesis of an inverse opal thin film of Ta_3N_5 produced through atomic layer deposition. The highly regular architecture achievable by atomic layer deposition is combined with an unusually high refractive index and transparency in at least part of the visible spectrum. The result is a material that represents the closest example to date of a photonic crystal with a band gap at optical wavelengths.

Introduction

Monodisperse colloidal particles have the ability to self-organize from a suspension of the colloids into ordered face centered cubic (fcc) arrays. Colloidal crystals, akin to the naturally occurring gem opal, diffract light at visible wavelengths because of the submicrometer diameter of the component particles. However, more remarkable photonic properties arise from the inverse opal architectures that can be generated using these colloidal arrays as templates.[1] The typical approach is to infiltrate the void space between the spheres of a colloidal crystal with the precursor(s) of the new material and to later remove the original particles.[2] This produces inverse opal architectures whose size and chemical composition are tunable by the size of the colloids and the infiltration precursor(s), respectively. When the dielectric constant of the matrix surrounding the air spheres is above a threshold value, inverse opals have been predicted theoretically and shown experimentally to be associated with a complete photonic band gap.[3−8] Light with wavelengths within the photonic band gap is not allowed to propagate through the material and is reflected from any direction by the photonic crystal.

A wide range of synthetic approaches have proved successful in creating inverse opal morphologies. Either latex or silica microspheres are typically used for the template because they are easy to prepare with narrow size distributions and with a wide range of precisely controlled submicrometer diameters. The two most common pioneering synthetic techniques used to generate inverse opal architectures were hydrolysis of sol−gel precursors to yield inorganic oxides[9−14] and polymerization of liquid monomers to yield several types of polymers.[14−18] Monodisperse emulsions have also been used as templates to generate titania inverse opals that retain structural integrity.[19,20] Other techniques, including electroless and electrochemical deposition and nanocrystal infiltration, extended the possible range of materials to both metallic[14,18,21,22] and semiconducting[23] inverse opal structures. As interest in this field grows, more approaches and synthetic variations have proved successful in the synthesis of inverse opals.[24] Chemical vapor deposition has been utilized to prepare carbon,[25] silicon,[8,26] and germanium[27] inverse opals.

More recently we have established the fundamentals of using atomic layer deposition (ALD) as an excellent new route to inverse opal morphologies with new versatility in the type of materials that can be used.[28] Atomic layer deposition is a film growth method characterized by alternate exposure of a templating substrate to gaseous chemical species.[29] The self-limiting nature of the alternating reactions ensures that the amount of material deposited at each exposure step is uniform and is limited by the chemisorption of a monolayer coating on the surface. As a result, ALD allows the deposition of films with exact thickness and composition control as well as remarkable uniformity and conformality.

The design of a photonic crystal with a complete photonic band gap (PBG) requires both a well-defined architecture and a large difference in the refractive indexes of its component materials. The PBG opens up at wavelengths that are of the same order as the periodicity in dielectric of the inverse opal system. This in turn is controlled by the diameter of the templating particles. In order for a complete PBG to appear in an fcc inverse opal crystal, the refractive index of the solid phase must be in excess of 2.8.[4] The solid should also be nonabsorbing at the band gap frequencies in order to avoid complications arising from electronic transitions. Despite these strict requirements, the ease of self-assembly associated with colloidal arrays has made this type of morphology the system of choice for the preparation of nonlithographic photonic materials. The predicted photonic properties for this system were proved by Vlasov et al. by preparing a silicon inverse opal system displaying a complete band gap.[8] Silicon's optical properties exceed the optical requirements discussed above in the near-IR, making it a suitable solid for synthesizing a photonic crystal with a band gap at those wavelengths.

Developing an inverse opal with a band gap at optical wavelengths requires particles with an average diameter of approximately 300−500 nm and, more challengingly, a transparent solid material providing sufficiently high refractive index.

* Corresponding authors. E-mail: tolbert@chem.ucla.edu (S.H.T.); gordon@chemistry.harvard.edu (R.G.G.).
[†] University of California Los Angeles.
[‡] Harvard University.

10.1021/jp047068b CCC: $30.25
Published on Web 12/13/2004

One of the very few solids that meets these optical requirements is the rutile phase of titania ($n \sim 3$). Synthetic efforts directed toward a titania inverse opal have failed to produce a photonic crystal with a complete band gap, however, in part due to the large size of the rutile crystallites and the inhomogeneity they introduced.[20] In addition, even infiltration of the interstitial spaces of a colloidal array is often hard to achieve using sol−gel precursors.

A new promising class of materials with refractive indexes of about 3 includes certain transition metal nitrides such as Zr_3N_4, Hf_3N_4, and Ta_3N_5. While considerable effort has gone into the development of the lower nitrides of zirconium, hafnium, and tantalum, much less is known about their higher nitrides mentioned above. Zirconium mononitride has received attention because of its high melting point and hardness and its chemical stability. It finds applications in hard and decorative coating materials, diffusion barrier materials, and thermally stable resistors. Nitride-rich Zr−N thin films have novel applications such as a cryogenic thermistor and as insulating films in a Josephson junction.[30] HfN and TaN have been applied as diffusion barriers because of their high conductivity, hardness, and melting point. While the metallic character of the lower nitrides makes them ideal for the above uses, the nonabsorbing properties of the semiconducting higher nitrides are of greater interest for optical applications. For example, in the case of tantalum, oxynitride materials such as TaON are applied to the detection of toxic metals and as gas sensors.[31,32] More recently, both TaON and Ta_3N_5 have been shown to be high efficiency photocatalysts for the oxidation of water.[33]

The fundamental interest in developing materials with a PBG in the visible range of the electromagnetic spectrum includes the suppression of spontaneous emission and the possible achievement of very long lived excited states. Technological impact has also been hypothesized in fields in which the inability of an excited species to decay radiatively enhances electron-transfer processes such as photocatalysis. In addition, in the presence of line defects along the photonic crystal, single molecule lasers and photon-based integrated circuits may be achieved by complete control of the direction of emitted photons from an excited species.

The goal of this work is thus to create a thin-film inverse opal material with a PBG at visible wavelengths. Here we extend our knowledge about infiltrating silica colloidal crystals by ALD to the deposition of a high index of refraction nitride that is nonabsorbing within a range of optical wavelengths. We developed a two-step synthesis of an inverse opal of Ta_3N_5, a semiconductor transparent in the red portion of the visible spectrum and with a high enough index of refraction (about 3) to have the potential to show a PBG.

Experimental Section

The silica particles were prepared by the Stöber method with the following modifications.[34] Tetraethoxyorthosilicate (TEOS) was hydrolyzed by small amounts of water in an ethanolic solution in the presence of ammonia. The reagents were mixed and stirred in a sealed plastic container for at least 3 h at room temperature. The amount of water and ammonia present in solution regulates the rates of nucleation and growth for the particles and ultimately affects their size. Incremental aliquots of TEOS and water were added to the reaction mixture to enhance the monodispersity of the population and increase the average diameter of the particles to the desired value of 429 nm ± 3%. Calculations of size and size distribution for the final population were obtained by measuring the size of at least 100 particles in transmission electron microscopy images.

The colloidal crystals were prepared by an established vertical deposition technique.[35,36] A quartz slide was held vertically in a 20 mL vial containing an ethanol suspension of 0.25−1.0 vol % particles. As the ethanol evaporates and the meniscus sweeps down the substrate, capillary forces induce ordering of the particles into a close-packed arrangement. Films were typically grown at a rate of 5−6 mm/day. For this study we prepared opal films with thickness ranging from 1.5 to 20 μm; most of the colloidal arrays had 10−20 layers of particles. This technique produces multilayered close-packed colloidal crystals that are firmly attached to the substrate. As the films dry and tend to shrink, however, the large crystalline domains tend to crack. This generates a collection of irregularly shaped islands about 5−10 μm in size. These islands are separated by a network of deep fractures perpendicular to the substrate that can be up to 2 μm wide.

In the preparation of tantalum nitride by ALD, pentakis(dimethylamino)tantalum ($Ta(N(CH_3)_2)_5$; PDMAT) and ammonia (NH_3) were used as precursors at 250 °C (Figure 1). Ta_2O_5 was deposited on colloidal silica substrates by alternating exposure to PDMAT vapor and water vapor at 250 °C (Figure 1). The reactor pressure was kept at 0.3 Torr by flowing high-purity nitrogen gas.[37] PDMAT was maintained at 90 °C to achieve the required vapor pressure, while water was kept at room temperature (25 °C). The sample was infiltrated with a dose of Ta precursor (0.7 μmol/cycle), followed by a dose of water (0.14 mmol/cycle). The dose of Ta precursor delivered to the substrate per unit area (as estimated by adding the surface area of reactor chamber and the internal surface area of colloidal substrate) was around 0.5 nmol/cm^2. The exposure to the tantalum precursor was about 6×10^3 langmuirs, which should be sufficient to infiltrate a straight hole with a length-to-diameter ratio of about 36:1.[38] The exposure to the water vapor was larger, so it should not limit the aspect ratio into which the coating can infiltrate.

The overlayer of Ta_2O_5-infiltrated colloidal crystals was etched using an Unaxis inductively coupled plasma (ICP) reactive ion etcher. The process gas was chlorine at 40 std cm^3/min and a pressure of 10 mTorr. The power of the ICP was 800 W and that of the RIE was 174 W. The samples were etched for 2−5 min and imaged to assess the extent of the etching process. The following wet etch was performed by gently soaking the samples in 1−2% HF(aq) for 2 min, rinsing with distilled water, and allowing the samples to air-dry.

Ta_2O_5 was converted to Ta_3N_5 by a nitridation reaction carried out in a reactor under flowing high-purity ammonia gas at about 1 atm and 800 °C for 2 h. Before heating the samples in the reactor, ammonia flowed through the chamber for 1 h. The rate of heating was 30 °C/min.

The samples were imaged at each stage of the process by scanning electron microscopy (SEM) using a Hitachi S4700. The need for a sputtered gold film was eliminated by mounting the quartz slide on adhesive carbon tacks and/or copper tape directly connecting the inverse opal structure to the aluminum mount. Optical images of the final inverse opal film were collected using the 20× or 100× objectives of a Leica microscope equipped with reflected illumination and a DC300 CCD. The film thickness and optical constants of Ta_2O_5 films on flat substrates were monitored with a Filmtek 2000 reflectometer made by SCI, Inc. The wavelength-dependent index of refraction and extinction coefficients of Ta_3N_5 were obtained using a Filmtek 3000 instrument by SCI, Inc. The wavelength dependence of the index of refraction is estimated to have an experimental error of about 5%, especially at wavelengths

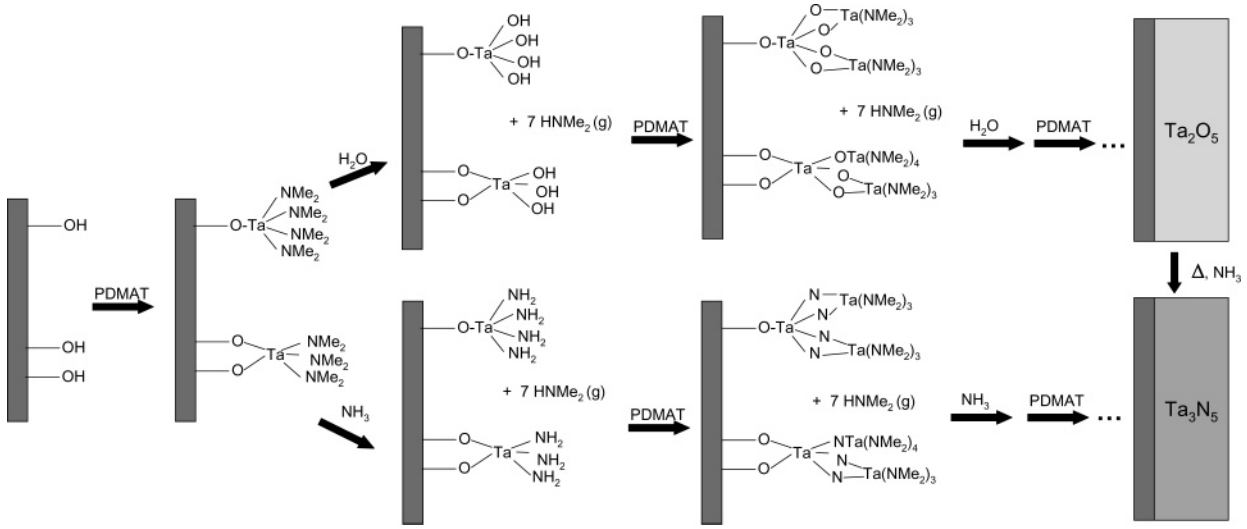

Figure 1. Reaction scheme for the deposition of Ta_2O_5 and Ta_3N_5 by ALD. The silanol groups of the templating silica surface react with PDMAT, the tantalum precursor, until the surface is saturated. After removal of unreacted PDMAT from the gas phase, a second precursor is allowed to react with the surface to complete the first cycle. The use of water (top branch) yields Ta_2O_5, while the use of ammonia (bottom branch) yields Ta_3N_5 in a similar fashion. In both cases dimethylamine is liberated from the surface at each step. While this approach produces a pure Ta_2O_5 film when water is employed, when ammonia is used the deposited film is a mixture of Ta_3N_5 and TaN. A pure Ta_3N_5 film may be prepared from a Ta_2O_5 film by means of high-temperature nitridation with ammonia gas.

shorter than about 610 nm due to the onset of a nonvanishing extinction coefficient. The reflectance of the Ta_3N_5 inverse opals was measured using the same instrument and a 50× objective to collect reflected light from a portion of the sample with a diameter of about 20 μm.

The theoretical reflectance spectra were calculated using Translight, software developed by Andrew L. Reynolds.[39] The fits to the experimental reflectance were optimized starting from the geometric parameters measured by SEM and the wavelength-dependent index of refraction of Ta_3N_5. The best fit to the reflectance spectra are were obtained with an index of refraction of 2.9, air holes of 411 nm diameter, and a shell thickness of 43 nm. These parameters are within the experimental error of the average measured values.

Results

In the nitride selection process, three nitrides were considered: Hf_3N_4, Zr_3N_4, and Ta_3N_5. Of these, Hf_3N_4 was discarded because its refractive index is the lowest of the three with a value of approximately 2.8. While Zr_3N_4 has a value of $n \sim 3.2$, its chemical resistance to the hydrofluoric acid required to dissolve the templating silica particles is unsatisfactory. Gaseous HF liberated from a dilute aqueous solution of hydrofluoric acid is enough to destroy a thin film of the solid. By contrast, Ta_3N_5, also with $n \sim 3.2$, was etched by aqueous HF much more slowly in preliminary experiments. Ta_3N_5 is a semiconductor that is virtually nonabsorbing at visible lengths longer than about 580 nm. This makes the material suitable for development of an inverse opal photonic crystal with a band gap in the red portion of the visible spectrum.

A schematic of the mechanism for the self-limiting surface reactions associated with the ALD process is presented in Figure 1. In the first step, the templating surface is saturated by the tantalum precursor PDMAT. Water or ammonia gas may be used as a precursor in the second step of each cycle to yield Ta_2O_5 or Ta_3N_5, respectively. On the basis of the known mechanism for similar precursors, PDMAT is believed to decompose via exchange reactions that liberate dimethylamine at each step.[40] While high-quality Ta_2O_5 films may be deposited in this fashion, preliminary experiments on the direct deposition of Ta_3N_5 on flat substrates or inside colloidal crystals by ALD using PDMAT and ammonia produced a material whose optoelectronic properties were not consistent with those of pure Ta_3N_5.[41] The material was black in color and conducted electricity consistent with contamination by the metallic lower nitride TaN. The presence of TaN was also confirmed by X-ray diffraction. Possible reasons for differences between the ALD of oxide and nitride include the high stability of TaN and the weaker nucleophilic nature of ammonia relative to the more reactive water molecules.

Therefore, a two-step synthetic approach was selected which first involved ALD of Ta_2O_5 followed by a nitridation reaction to yield pure, transparent Ta_3N_5. The overall inverse opal synthesis (shown schematically in Figure 2) thus encompassed the infiltration of the colloidal crystal with Ta_2O_5 followed by etching to remove the templating particles. The final step was the conversion of the Ta_2O_5 inverse opal to the final Ta_3N_5 photonic crystal.

The optoelectronic quality of the Ta_3N_5 that could be prepared by this method was tested on films deposited on flat substrates that had undergone the same chemical transformations as the ones employed in the preparation of the photonic crystal. Flat films of Ta_2O_5 on a quartz substrate were converted to Ta_3N_5, and the wavelength-dependent index of refraction and extinction coefficient were calculated from reflectance and transmission measurements. As can be seen in Figure 3, in the region of the visible spectrum where Ta_3N_5 is transparent (~580−750 nm), the index of refraction is in excess of the value of 2.8 required to observe a PBG.

The chemical resistances of both Ta_3N_5 and Ta_2O_5 to hydrofluoric acid were tested to ensure that their etching rates were slow enough to allow for the dissolution of the silica particles without compromising the Ta_2O_5 inverse opal architecture. Even though the initial selection of Ta_3N_5 was based on its resistance to etching by HF, Ta_2O_5 appears to be even more inert in this respect. Flat films of Ta_2O_5 were deposited on silicon wafers and etched for variable amounts of time with 10% aqueous HF. The measured etch rates were 4 nm/min for Ta_3N_5 and 0.5 nm/min for Ta_2O_5; the latter etch rate is more than 1 order of magnitude slower than that of silica. In addition,

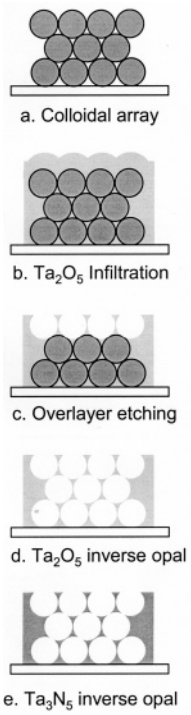

Figure 2. Scheme of Ta_3N_5 inverse opal preparation. A thin-film colloidal crystal (a) is infiltrated with Ta_2O_5 using ALD. The resulting filled structure shows an undulated overlayer (b). The overlayer and the top monolayers of particles are removed by RIE (c). The rest of the particles are eliminated with aqueous HF resulting in a Ta_2O_5 inverse opal (d). This architecture is converted to the final Ta_3N_5 inverse opal (e) crystal by means of a high-temperature nitridation reaction in ammonia gas.

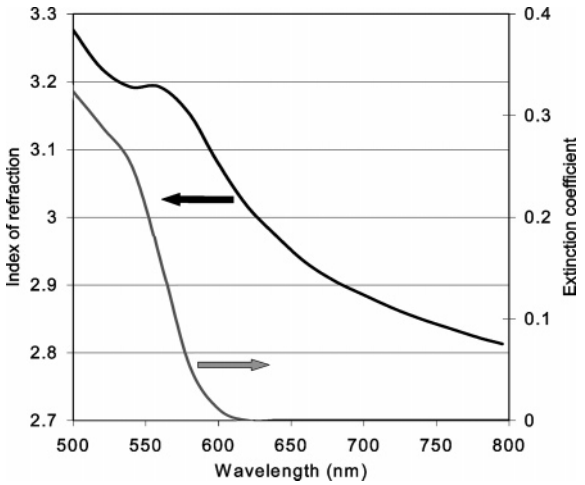

Figure 3. Wavelength-dependent index of refraction and extinction coefficient for Ta_3N_5. At wavelengths longer than approximately 600 nm, this material is transparent but still has the high value of index of refraction required to observe a full PBG.

exposure of Ta_2O_5 to HF results in no chemical changes that prevent its later conversion to Ta_3N_5 with optical constants equal to the ones mentioned above (Figure 3). In contrast, HF etching in the case of Ta_3N_5 appears to be associated with a small decrease of its index of refraction as well as the film thickness, likely as a result of oxidation.

At the end of the Ta_2O_5 infiltration process, all the surfaces of the colloidal crystal are coated with the deposited solid. This means that, in addition to infiltrating the internal surface area of the crystal, an overlayer of a few tens of nanometers of solid Ta_2O_5 is frequently observed on the top surface and along the sides the cracks separating the different islands of the colloidal crystal (Figure 4a).[28] In order to access the silica particles and dissolve them using hydrofluoric acid, it is useful to remove enough of this overlayer from the top surface to expose the first monolayer of particles and facilitate the access to the inner network by the wet etching agent. This was achieved by controlling the conditions of a reactive ion etching (RIE) process in order to expose the first layer of particles only. Even under conditions where the overlayer is only partially removed (as shown in Figure 4b), RIE results in the removal of the first few layers of particles deep into the crystal, most likely as a result of the enhanced etching rate of silica relative to Ta_2O_5 under these conditions. The colloidal particles buried deeper inside the crystal were dissolved by soaking the sample in 1−2% aqueous HF for 2 min. This treatment also results in the removal of any residual overlayer that survived the RIE step (Figure 4c).

The nitridation of Ta_2O_5 inverse opals was carried out by flowing ammonia gas over the films at 800 °C in analogy to several reports of the nitridation of Ta_2O_5 to yield Ta_3N_5.[42−45] At the end of this step the inverse opal changed in color from pale yellow to bright orange, in accordance with the known absorbance spectrum of Ta_3N_5 (Figure 3).[41] In consideration of the slower etch rate of Ta_2O_5 relative to Ta_3N_5 discussed earlier, the choice was made to dissolve the silica particles before the nitridation to avoid damage to the final nitride inverse opal by hydrofluoric acid. This approach has the added benefit of facilitating the diffusion of ammonia gas within the porous architecture of the crystal during the nitridation step.

The colloidal crystals used in this study were prepared from silica particles with an average diameter of 429 nm. The inverse opal films have air holes with a slightly smaller diameter of 411 nm, produced as a consequence of particle shrinkage associated with the elevated temperatures in the ALD chamber.[28] Most of the crystal is aligned with the (111) planes parallel to the substrate (Figure 4d,e), although smaller domains with (100) orientation are also present (Figure 4f). The Ta_3N_5 shell thickness was approximately 43 nm, in perfect agreement with other inverse opals prepared by gas-phase techniques. No measurable changes in the architectural parameters are apparent from the SEM micrographs upon conversion of the Ta_2O_5 inverse opal to Ta_3N_5.

Figure 5 shows typical images collected from the sample using an optical microscope in reflection. Different areas of the samples appear different in color and brightness: a good fraction of the film is red/brown in color as shown in Figure 5a, while many other portions of the film are much brighter and white to yellow in color as shown in Figure 5b. The gaps associated with drying that separate the different islands of the original colloidal crystal are clearly visible in both instances.

Reflectance spectra of the brighter areas of the photonic crystal (similar to the ones shown in Figure 5b) are shown in Figure 6 and are presented with calculated reflectance spectra. The quantitative knowledge of the geometric details of the inverse opal architecture and of the optical constant of Ta_3N_5 allow for a theoretical calculation of the wavelength-dependent reflectance for the sample along any given direction for the lattice. The calculated reflectance spectra along the (111) and (100) directions are included in Figure 6a and Figure 6b, respectively.

Discussion

The exact photonic properties of inverse opal system depend subtly on a combination of its geometric parameters (e.g., the diameter of the air spheres and the thickness of the shells of

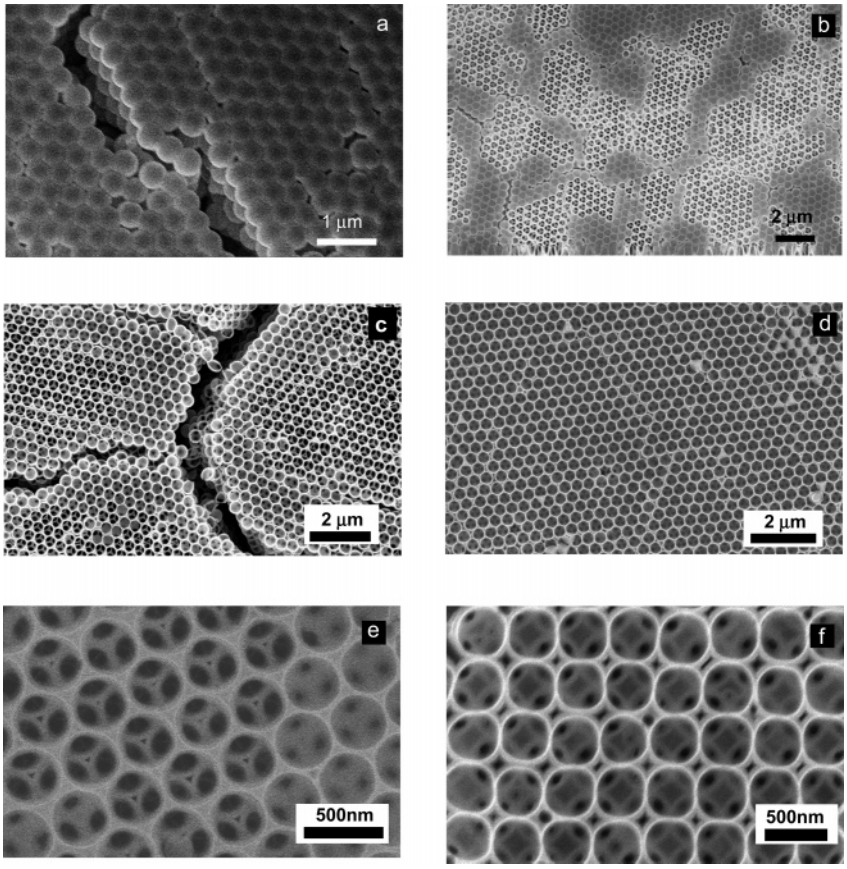

Figure 4. SEM images of sample at each stage of the synthesis. (a) The colloidal array at the end of the Ta_2O_5 infiltration by ALD. The undulated top surface results from the conformal growth of an overlayer. A gap separating two islands in the sample is also visible. (b) The overlayer and templating particles in the top monolayers are removed by RIE. (c) Dilute HF completes the removal of the overlayer and dissolves the remaining templating particles. The Ta_2O_5 inverse opal structure can be converted to Ta_3N_5 (d) with no change in structure. The final crystal has a predominant (111) orientation (d and e) with a smaller proportion of domains that are (100) oriented (f).

solid surrounding them) and of the optical constants of the solid material that forms the inverse opal. Because their propagation through the crystal is not allowed, complete reflectance is predicted for photons with wavelengths within the PBG of the photonic crystal lattice. While the exact width and position of the band gaps along different lattice directions vary, a complete PBG result occurs for these systems from the overlap of band gaps along all lattice directions. Because the vast majority of the domains in our thin-film colloidal array are oriented with their (111) planes parallel to the substrate, however, this is the most easily accessed direction for spectroscopic measurements.

As discussed earlier, a high index of refraction is a key factor for a PBG to open up. Therefore, this is generally a parameter that is fixed (hopefully at a maximum value) by choosing an appropriate nonabsorbing material (Ta_3N_5 in our case). Conversely, many of the geometric parameters of the inverse opal architecture can be tuned in such a way that the width of the PBG is maximized and its exact center position is selected to fall within a certain range. For example, in the case of Ta_3N_5 and its optical constants (Figure 3), it can be calculated that along the (111) direction the maximum band gap width will occur for a system of air spheres with a diameter of about 400 nm. Therefore, because the templating silica particles experience shrinkage when heated in the ALD chamber, a colloidal array was prepared from particles of about 430 nm average diameter.

As we mentioned, the photonic properties of an inverse opal are very sensitive to its architecture as well as any structural inhomogeneity or defects. Because most deviations from the ideal arrangement in the final architecture are transferred from the colloidal crystal template, it is useful to discuss the

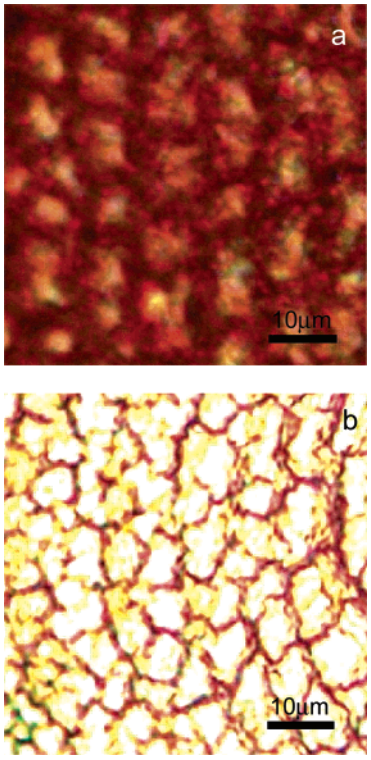

Figure 5. Optical images of (a) darker and (b) brighter portions of the sample. The gaps separating the islands of the films are visible in both instances. The areas of the films that appear bright yellow/white in color, i.e., region (b), are associated with photonic properties matching the theoretical reflectance spectra calculated for this system.

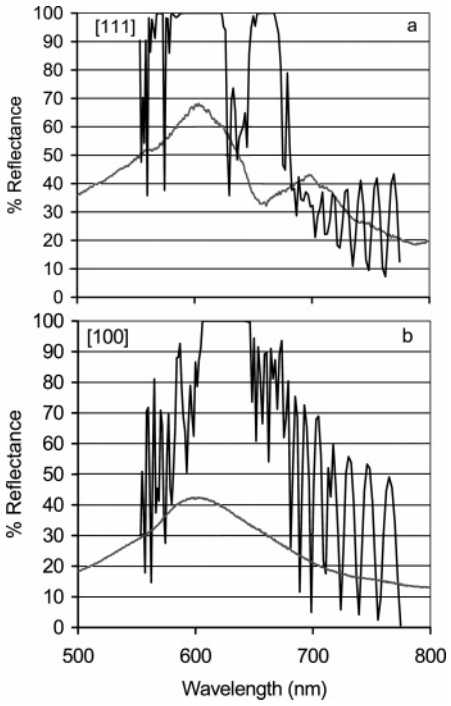

Figure 6. Theoretically calculated (black) and experimentally measured (gray) reflectance spectra of the brightest areas from the Ta_3N_5 inverse opal. (a) The spectra associated with the prevalent (111) orientation show the characteristic two-peak pattern corresponding to the two photonic band gaps predicted by calculation. (b) The single peak along the (100) direction at about 600 nm overlaps with the primary gap along the (111) direction and determines the position of the PBG for this system.

template's imperfections. When grown by the vertical deposition technique utilized here, thin-film colloidal arrays achieve the highest density of particles along the substrate and tend to form with the (111) planes parallel to it. Occasional small domains with (100) orientation appear as square lattice domains (Figure 4f) surrounded by the prevalent hexagonal lattice (Figure 4d,e). Observation of the hexagonal lattice of the top surface reveals that the array tends to be a single crystal although line defects tend to separate domains of tens to hundreds of micrometers that may be slightly out of registry.[18] More importantly, as the colloidal array dries from the alcohol suspension that forms it and is subsequently heated in the ALD chamber, the film cracks giving rise to islands 5−20 μm wide separated by about 2 μm gaps.[28]

The following steps of the synthesis make smaller contributions to the imperfection of the Ta_3N_5 inverse opal. A highly conformal film of the solid is formed on the surface of all particles making up the array because of the self-limiting nature of the ALD reactions. Earlier results show that the thickness of the shells is the same whether the shells are near the top surface of the film or deeper and closer to the substrate.[28] Indeed, infiltration of the colloidal array by ALD produces very regular architectures that are optimal for a photonic crystal. In the course of the ALD cycles as the film thickness increases, a small portion of the empty space becomes inaccessible to the gaseous precursors, resulting in small tetrahedral pores between each set of four spheres. In fact, this architecture, which is best described as a close-packed arrangement of hollow shells, has been predicted to result in an enhanced photonic crystal with a wider PBG relative to a fully infiltrated structure lacking these small tetrahedral pores.[4] The overlayer observed on the top surface of the film represents the only undesirable deviation from an ideal architecture. The surface of the overlayer appears as periodic undulations due to the replication of the surface features by the conformal growth of the solid (Figure 4a).[28] Utilizing the absolute minimum number of cycles required to fully infiltrate the internal surface of the colloidal crystal may minimize the thickness of this overlayer and facilitate its removal by wet etching techniques alone. On the other hand, the elimination of the overlayer is straightforward using RIE techniques.

While the rate of etching of Ta_2O_5 by HF is much slower than that of silica, a certain degree of inhomogeneity in the architectures may be introduced by the removal of the silica spheres. The need for the hydrofluoric acid solution to diffuse through the tortuous network left behind by the dissolving particles may result in only a partial etching of the colloids in the layers of the array closest to the substrate. Conversely, harsher etching conditions may be associated with excessive etching of the inner surface of each Ta_2O_5 shell, resulting in thinner shells of the material close to the top of the film relative to the ones closer to the substrate. In addition, the incomplete removal of the overlayer by RIE may result in thicker shells for the portions of the film still protected by the overlayer at the beginning of the wet etching process. Figure 4e supports this idea as it shows thicker shells on the right-hand side of the image, as evidenced by smaller channels connecting each air hole to its nearest neighbors.

The last step of the photonic crystal synthesis, the conversion of the Ta_2O_5 inverse opal to the Ta_3N_5 inverse opal, does not appear to compromise the integrity of the architecture or affect its morphology in any measurable way, despite the high temperatures used (Figure 4). This result is in agreement with very recent results on the nitridation of Ta_2O_5 particles to Ta_3N_5 showing that, while no change in the size of the particles is associated with the transformation, the final Ta_3N_5 particles display some porosity.[46] Our data do not directly indicate the emergence of porosity within the Ta_3N_5 shells of the final photonic crystal. The presence of pores would, however, result in a lower than expected refractive index for the nitride material, which may be an explanation of why the best fit to the reflectance spectra is achieved with the slightly low value of 2.9.

The most useful characterization of the photonic properties of the final inverse opal comes from the optical imaging and the reflectance spectra of different areas of its surface. The optical images reveal areas of the film with different colors and brightness as a consequence of different reflectance spectra associated with different portions of the surface. Portions of the film with low reflectance that are red to brown in color, such as the area shown in Figure 5a, indicate that at these locations the inverse opal architecture is too irregular to display a PBG. This is likely due to inhomogeneity in the structure of the films due to the etching process such as the ones discussed above. More specifically, we believe this to be the consequence of the presence of a decreasing gradient of thickness from the substrate to the top surface of the film of the Ta_3N_5 shells due to increased etching of the inner surfaces of the Ta_2O_5 spherical shells. The high sensitivity of the wavelength of the PBG to small variations in shell thickness would result in a superposition of slightly overlapping PBGs associated with different layers of the films, ultimately resulting in loss of the reflectance properties for this imperfect photonic crystal. By the same token, this result suggests that, under conditions where the HF treatment can be more carefully controlled, etching itself is a viable way to tune the position of the PBG by altering the geometric parameters of the lattice in the course the synthesis.

The presence of bright portions of the film, such as the one shown in Figure 5b, is an indication that our approach is successful in preparing quality photonic crystals even in the absence of controlled etching conditions. The reflected luminosity of these areas corresponds to the reflectance spectra shown in Figure 6a and Figure 6b showing the expected features for domains with (111) and (100) orientation, respectively, as observed by SEM (Figure 4d,f). The theoretical reflectance spectra expected for an fcc inverse opal depend on the incident angle of the light with the respect to the lattice places of the crystal. The finite overlap of wavelengths for which total reflectance is measured irrespective of direction corresponds to the complete PBG.

The spectrum shown in Figure 6a reveals the presence of two reflectance peaks, a more intense one at 605 nm and a less intense one at about 700 nm. As is shown by a theoretical calculation of the reflectance spectra also in Figure 6a, the expected reflectance for the (111) direction of this photonic crystal does include two band gaps of different widths centered around the same wavelengths as those observed experimentally. Figure 6b shows the same type of data but displays the single reflectance peak associated with the (100) orientation of the lattice, also in accord with the theoretical calculation. This peak is observed at about 600 nm, and it thus overlaps with the primary peak of the (111) direction marking the position of the potential three-dimensional PBG of this crystal. In the case of the (111) direction, the wavelength of the primary peak at 605 nm is in better agreement with the theoretical calculation than the narrower secondary peak at longer wavelength. Similarly poor agreement has been observed by other researchers,[8] suggesting that it may simply be a consequence of imperfections associated with the model used for the calculations. In surveying the surface of sample, the transmission spectra showing the two peaks associated with the (111) direction were far more common than the (100) one-peak spectrum. It was also not uncommon for certain areas to show a superposition of the two types of spectra as a consequence of interspersion of small domains with sizes smaller than the cross section of the impinging light beam.

As mentioned earlier, the presence of a complete PBG is associated with 100% reflectance of wavelengths falling within the gap range. The presence of drying cracks (clearly visible in Figure 5) has an important consequence on our ability to measure the absolute reflectance of the sample. Because the gaps run vertically all the way down to the substrate, this type of defect is among the most detrimental to the measurement of the photonic properties of the final inverse opal in the direction normal to the substrate. It is expected that the vertical gaps in the film will allow some of the light impinging on the sample to propagate undisturbed toward the quartz substrate and not be reflected by the photonic crystal even if its wavelength falls within the PBG. Because the size of the probing beam is significantly larger than the size of individual sample islands, it is difficult to characterize fully the photonic properties of the material. Care was taken to limit the spot size of the impinging light beam and of the reflected cone to avoid the vertical gaps. Unfortunately, even when spectra were collected using a beam with a cross section as small as about 20 μm, it was not possible to avoid these structural defects and eliminate their contribution. We believe this to be the main reason the intensity of the reflectance peaks only approach but do not coincide with the 100% reflectance predicted in the case of an ideal PBG crystal. Even if the intensity of reflectance peaks is diminished by the presence of drying gaps, the spectral patterns illustrated in Figure 6 are a clear indication that the methods described in this work can be optimized for the production of an inverse opal photonic crystal based on Ta_3N_5 with a PBG in the visible.

Conclusions

In this work we describe the synthesis of an inverse opal thin-film colloidal crystal of Ta_3N_5 and report on its photonic properties. Silica particle colloidal arrays are used as templates in a two-step synthesis based on their infiltration with Ta_2O_5 by atomic layer deposition and the conversion of Ta_2O_5 to the final Ta_3N_5 inverse opal structure by a nitridation reaction. The size of the features of the inverse opal and the PBG associated with it can be controlled by the size of the templating colloids, the thickness of the solid deposited by ALD, and the extent to which features are etched with HF. The photonic crystal prepared by this method displays a preponderance of domains with (111) lattice planes parallel to the substrate and a minority that have (100) orientation. The drying cracks of the samples diminish our ability to measure the complete reflectance associated with a full PBG. However, the patterns of the measured reflectance spectra are in excellent agreement with calculations based on the structural parameters and the optical constants for this material, indicating that our proposed method is suitable for the development of the first reported material with a PBG at optical wavelengths.

The development of photonic materials is regarded as a powerful approach to control the emission and propagation of light. The route to a PBG at visible wavelengths presented here is optimized for thin-film samples and relies on techniques that are common in the semiconductor industry. Because the full photonic effect in these systems is achieved with just a few layers,[47] miniaturization of the crystal could minimize the films' shrinkage cracks and other defects while maintaining the desired properties. This suggests that our approach may represent an important innovation in controlling the flow of visible light with great potential to lead toward applications such as bright LEDs and low-threshold lasers.

Acknowledgment. The authors are deeply thankful to Dr. Jill S. Becker for her contribution to the initial stages of the project and Dr. Antti Rahtu, who was instrumental in identifying the need for the alternative two-step synthesis of Ta_3N_5 presented here. The help of Dr. Chris Claypool of SCI, Inc., in measuring the optical constants of Ta_3N_5 and the reflectance spectra of the samples is gratefully acknowledged. This work was supported by the Office of Naval Research under Grant N00014-99-1-0568, by the National Science Foundation, and by the Beckman Foundation. S.H.T. is an Alfred P. Sloan Foundation Research Fellow.

References and Notes

(1) Velev, O. D.; Jede, T. A.; Lobo, R. F.; Lenhoff, A. M. *Nature* **1997**, *389*, 447. Velev, O. D.; Jede, T. A.; Lobo, R. F.; Lenhoff, A. M. *Chem. Mater*. **1998**, *10*, 3597.

(2) Velev, O. D.; Kaler, E. W. *Adv. Mater*. **2000**, *12*, 531.

(3) Yablonovitch, E. *J. Opt. Soc. Am. B* **1993**, *10*, 283. Yablonovitch, E.; Gmitter, T. L. *Phys. Rev. Lett*. **1989**, *63*, 1950.

(4) Busch, K.; John, S. *Phys. Rev. E* **1998**, *58*, 3896.

(5) Ho, K. M.; Chan, C. T.; Soukoulis, C. M. *Phys. Rev. Lett*. **1990**, *65*, 3152.

(6) Biswas, R.; Sigalas, M. M.; Subramania, G.; Ho, K. M. *Phys. Rev. B* **1998**, *57*, 3701.

(7) Moroz, A.; Sommers, C. *J. Phys.: Condens. Matter* **1999**, *11*, 997.

(8) Vlasov, Y. A.; Bo, X.-Z.; Sturm, J. C.; Norris, D. J. *Nature* **2001**, *414*, 289.

(9) Imhof, A.; Pine, D. J. *Nature* **1997**, *389*, 948.

(10) Holland, B. T.; Blanford, C. F.; Stein, A. *Science* **1998**, *281*, 538. Holland, B. T.; Blanford, C. F.; Do, T.; Stein, A. *Chem. Mater.* **1999**, *11*, 795. Holland, B. T.; Abrams, L.; Stein, A. *J. Am. Chem. Soc.* **1999**, *121*, 4308.

(11) Wijnhoven, J. E. G.; Vos, W. L. *Science* **1998**, *281*, 802.

(12) Yin, J. S.; Wang, Z. L. *Adv. Mater.* **1999**, *11*, 469.

(13) Yang, P. D.; Deng, T.; Zhao, D. Y.; Feng, P. Y.; Pine, D.; Chmelka, B. F.; Whitesides, G. M.; Stucky, G. D. *Science* **1998**, *282*, 2244.

(14) Jiang, P.; Bertone, J. F.; Colvin, V. L. *Science* **2001**, *291*, 453.

(15) Park, S. H.; Xia, Y. N. *Chem. Mater.* **1998**, *10*, 1745. Park, S. H.; Xia, Y. N. *Adv. Mater.* **1998**, *10*, 1045.

(16) Gates, B.; Yin, Y.; Xia, Y. N. *Chem. Mater.* **1999**, *11*, 2827.

(17) Johnson, S. A.; Ollivier, P. J.; Mallouk, T. E. *Science* **1999**, *283*, 963.

(18) Jiang, P.; Cizeron, J.; Bertone, J. F.; Colvin, V. L. *J. Am. Chem. Soc.* **1999**, *121*, 630.

(19) Subramanian, G.; Manoharan, V. N.; Thorne, J. D.; Pine, D. J. *Adv. Mater.* **1999**, *11*, 1261.

(20) Manoharan, V. N.; Imhof, A.; Thorne, J. D.; Pine, D. J. *Adv. Mater.* **2001**, *13*, 447.

(21) Yan, H. W.; Blanford, C. F.; Holland, B. T.; Parent, M.; Smyrl, W. H.; Stein, A. *Adv. Mater.* **1999**, *11*, 1003.

(22) Velev, O. D.; Tessier, P. M.; Lenhoff, A. M.; Kaler, A. M. *Nature* **1999**, *401*, 548.

(23) Braun, P. V.; Wiltzius, P. *Nature* **1999**, *402*, 603.

(24) Many examples are included in the special issue of: *Adv. Mater.* **2001**, *13* (6).

(25) Zakhidov, A. A.; Baughman, R. H.; Iqbal, Z.; Cui, C.; Khayrullin, I.; Dantas, S. O.; Marti, J.; Ralchenko, V. G. *Science* **1998**, *282*, 897.

(26) Miguez, H.; Tetreault, N.; Yang, S. M.; Kitaev, V.; Ozin, G. A. *Adv. Mater.* **2003**, *15*, 597.

(27) Meseguer, F.; Blanco, A.; Miguez, H.; Garcia-Santamaria, F.; Ibisate, M., Lopez, C. *Colloids Surf.* **2002**, *202*, 281.

(28) Rugge, A.; Becker, J. S.; Gordon, R. G.; Tolbert, S. H. *Nano Lett.* **2003**, *3*, 1293.

(29) Suntola, T. *Mater. Sci. Rep.* **1989**, *7*, 266.

(30) Inoue, S.; Tominaga, K.; Howson, R. P.; Kusaka, K. *J. Vac. Sci. Technol., A* **1995**, *13*, 2808.

(31) Gouin, X.; Marchand, R.; Laurent, Y.; Gervais, F. *Solid State Commun.* **1995**, *93*, 857.

(32) Le Gendre, L.; Piriou, Marchand, R. *Eur. J. Solid State Inorg. Chem.* **1997**, *34*, 973.

(33) Hitoki, G.; Takata, T.; Kondo, J. N.; Hara, M.; Kobayashi, H.; Domen, K. *Chem. Commun.* **2002**, 1698. Hitoki, G.; Ishikawa, A.; Takata, T.; Kondo, J. N.; Hara, M.; Domen, K. *Chem. Lett.* **2002**, *7*, 736. Hara, M.; Hitoki, G.; Takata, T.; Kondo, J. N.; Kobayashi, H.; Domen, K. *Catal. Today* **2003**, *78*, 555.

(34) Bogush, G. H.; Tracy, M. A.; Zukoski, C. F., IV. *J. Non-Cryst. Solids* **1988**, *104*, 95.

(35) Dimitrov, A. S.; Nagayama, K. *Langmuir* **1996**, *12*, 1303.

(36) Jiang, P.; Bertone, J. F.; Hwang, K. S.; Colvin, V. L. *Chem. Mater.* **1999**, *11*, 2132.

(37) Becker, J. S.; Gordon, R. G. *Appl. Phys. Lett.* **2003**, *82*, 2239.

(38) Gordon, R. G.; Hausmann, D. M.; Kim, E.; Shepard, J. *Chem. Vap. Deposition* **2003**, *9*, 73−78.

(39) http://www.elec.gla.ac.uk/groups/opto/photoniccrystal/Software/SoftwareMain.htm.

(40) Ritala, M.; Leskelä, M. *Chem. Mater.* **1994**, *8*, 556. Leskelä, M.; Ritala, M. *Thin Solid Films* **2002**, *409*, 138.

(41) Chun, W.-C.; Ishikawa, A.; Fujisawa, H.; Takata, T.; Kondo, J. N.; Hara, M.; Kawai, M.; Matsumoto, Y.; Domen, K. *J. Phys. Chem.* **2003**, *107*, 1798.

(42) Houmes, J. D.; zur Loye, H.-C. *J. Solid. State Chem.* **1996**, *127*, 267.

(43) Brauer, G.; Weidlein, J. R.; Straehle, J. *Z. Anorg. Allg. Chem.* **1966**, *348*, 298.

(44) Swisher, J. H.; Read, M. H. *Metall. Trans.* **1972**, *3*, 489.

(45) Brauer, G.; Weidlein, J. R. *Angew. Chem.* **1965**, *77*, 218.

(46) Lu, D.; Hitoki, G.; Katou, E.; Kondo, J. N.; Hara, M.; Domen, K. *Chem. Mater.* **2004**, *16*, 1603.

(47) Bertone, J. F.; Jiang, P.; Hwang, K. S.; Mittleman, D. M.; Colvin, V. L. *Phys. Rev. Lett.* **1999**, *83*, 300. Bertone, J. F.; Mittleman, D. M.; Jiang, P.; Hwang, K. S.; Colvin, V. L. *J. Chem. Phys.* **1999**, *111*, 345.